Interactive Visual Optimization of SPECT Prereconstruction Filtering

Michael A. King, Stephen J. Glick, Bill C. Penney, Ronald B. Schwinger, and Paul W. Doherty

Department of Nuclear Medicine, The University of Massachusetts Medical Center, Worcester, Massachusetts

A number of factors must be considered when forming a digital filter to two-dimensionally filter single photon emission computed tomographic (SPECT) acquisition images. In an effort to provide subjectively optimal filtering, a program has been developed which provides "real-time" visual feedback. This allows a user to select from among a family of Metz filters tailored for the imaging conditions (i.e., formed to deconvolve scatter, septal penetration, and combined collimator and intrinsic spatial resolution losses). Also, a guideline for assisting the user in selecting from among the possible Metz filters has been formulated. This guideline is based upon knowledge of the probability distribution of the noise power spectrum, and consists of choosing the filter which has a value of 1.0 when the one-dimensional compression of the image power spectrum equals the 90% confidence limit for noise fluctuations. The program starts by filtering a planar reference image with the Metz filter computed for the radionuclide, collimator, magnification, and count-level of the image. This filter is displayed beside the image where it is overlayed on a plot of the logarithm of the one-dimensional compression of the image power spectrum. The user is then allowed to vary the filter parameters through movement of a joystick. By doing the filtering using an array processor, a new filtered image is formed and displayed less than a second after movement of the joystick. Visual feedback from the series of filtered images thus produced as well as the plots of the filter overlayed on the estimated blurred object power spectrum are used to obtain a visually "optimal" filter. The filter can be adapted to the visual preferences of the individual reader, and serves as a useful teaching tool on the effects of filtering.

A significant improvement in the quality of single photon emission computed tomographic (SPECT) images has been demonstrated through the use of two-dimensional prereconstruction filtering of the SPECT projection (or acquisition) images (*1–5*). To obtain the maximum restoration of image quality, the restoration filter should be designed to account for the image blurring [modulation transfer function (MTF)], the noise level, and the object which was imaged (*1–6*). Using the normalized mean square error as the optimization criterion, and images of the Alderson Organ Scanning Phantom with liver and spleen inserts, a count-dependent Metz filter has been previously developed for use in two-dimensional prereconstruction fil-

tering the SPECT liver and spleen studies (*1*). This filter has been "optimized" for a number of imaging conditions (MTFs) (*4,5*). However, it was noted that alteration of the filter parameters from those determined from the phantom studies was required to obtain the most visually pleasing images for organ systems (objects) which were quite different from the liver and spleen studies for which the filter was optimized.

This paper describes a method which uses interactive visual feedback (*7–9*) to allow an operator to select from among a family of "optimal" Metz filters (i.e., those designed for a particular MTF) the filter best suited for the image being processed (i.e., object imaged and noise level). The visual feedback comes from two sources. The first is the viewer's subjective impression of image quality (*7–9*). The second comes from a plot of the frequency-domain filter overlayed onto the one-dimensional compression of a smoothed estimate of the power spectrum of the blurred object. We have observed

for SPECT studies that adjusting the Metz filter so that it has a value of 1.0 when the blurred object power spectrum equals the 90% confidence limit for fluctuations in the noise power spectrum generally produces images which are close to those interactively chosen by the users.

METHODS

Use of Image Power Spectrum in Filter Design

In the frequency domain, a digital filter is a sequence of numbers which are multiplied with the frequency content of an image (its Fourier transform) during the process of filtering. In this way, the filter sifts the frequency content of an image such that each component is enhanced (filter term greater than 1.0), passed unaltered (filter term equal to 1.0), attenuated (filter term less than 1.0), or completely removed (filter term equal to 0.0). Each component of the image in the frequency domain consists of a real and an imaginary part. The relative magnitudes of each of these determines the phase angle of the component (or angular offset from zero degrees of the cosine term represented by the component). In image processing, it is well known that the phase of the Fourier transform of an image is more important than the magnitude (11). In the restoration filtering of nuclear medicine images it is usually assumed that the camera does not, on the average, shift the position of counts and that the line spread functions are symmetric. This results in the magnitudes of the frequency terms being altered but not the phase angles. Thus restoration filters are generally based on the imaging system MTFs and not the optical transfer functions (OTFs) which include phase information. If one was to try to restore the image for patient motion for instance, then the inclusion of phase information in the filter would be necessary (12). Restoration filters generally follow the inverse of the MTF up to some point which is image specific and then smoothly decrease toward zero to avoid unduly amplifying frequency components which are dominated by noise (1-6).

This observation can be understood by analyzing the image power spectrum. The image power spectrum portrays the relative distribution of power among the frequency components of the image (13). It can be modeled as consisting of the sum of the power spectrum of the blurred object (the object as altered by the MTF during acquisition) and the power spectrum of the noise. It has been shown that for images degraded by Poisson noise, the power spectrum of the noise fluctuates around a constant mean value equal to the total count (6,14,15). Since the blurred object power spectrum generally decreases with frequency, a point is reached where the noise power spectrum becomes significant compared to that of the blurred object. The frequency at which this transition occurs depends upon the count level, the object being imaged, and the MTF (1,3-6,9,10). Designing a filter by visually determining when the noise first becomes significant compared to the blurred object can provide an important key to optimal filter design (3,10).

In the present work, this key is provided by presenting the operator with a display of the processed image and the logarithm of the one-dimensionally compressed image power spectrum after subtraction of the average noise level (i.e., the estimated blurred object power spectrum) and filtering with

an equally weighed three-point filter (i.e., three-point moving average). The present Metz filter is displayed overlayed onto the plot of this estimated spectrum. A horizontal reference line is displayed at a filter level of 1.0 and a second horizontal reference line is displayed at the 90% confidence limit of the fluctuations in the noise power spectrum. Since the individual terms of the two-dimensional noise power spectrum follow a Chi-squared distribution with two degrees of freedom (13,16), the 90% confidence limit is 2.3 times the mean value of the noise power spectrum. This value was checked using twenty-five 128 by 128 pixel images and it was determined that an average of 9.9% (s.d. of 0.4%) of the individual frequency terms exceeded this value at frequencies where noise dominates the image power spectrum. A joystick is used to vary the count-level for which the Metz filter (17) is formed and, hence, the shape of the filter while visually watching the overlayed curves and the restored image. We have observed at the count level of SPECT acquisition images that generally the most visually pleasing planar images (and SPECT slices reconstructed from them) result when the Metz filter is ~1.0 when the blurred object power spectrum first equals the 90% confidence limit for fluctuations in the noise power spectrum. This heuristic guideline means that the filter is adjusted to have a value of 1.0 when there is a 10% chance it would be otherwise amplifying frequency terms where the noise dominates the object.

Count-Dependent Metz Filter

The restoration filter selected for visual optimization was the count-dependent Metz filter (1,4,5,17). The one-dimensional frequency domain form of the Metz filter is defined as (18,19):
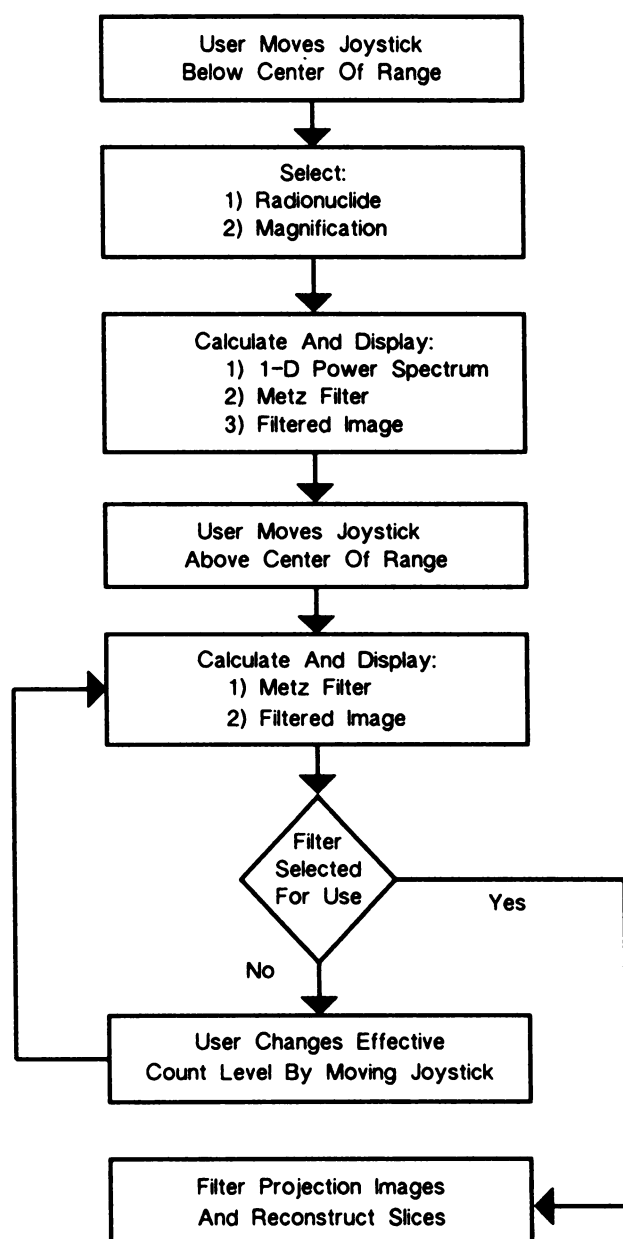
$$M(f) = MTF(f)^{-1} \cdot [1 - (1-MTF(f)^2)^X],\qquad(1)$$

where f is the spatial frequency, MTF is the modulation transfer function, and X is a factor which controls the extent to which the inverse filter [first term on right of Eq. (1)] is followed before the low-pass portion of the filter (second term) dominates. The parameters of the Metz filter were optimized using images of the Alderson Organ Scanning Phantom with liver and spleen inserts and minimizing the normalized mean-squared error (NMSE) as the optimization criterion.

Advantage is taken of the count-dependent behavior of the Metz filter by giving the user joystick control over the total count used to form the filter. The joystick is set so that when it is in the center of its range, the actual count is used. When the joystick is moved up or down, the count is increased or decreased, respectively, by a fractional power of 2.

Implementation

Figure 1 provides a flow chart of the visual filter optimization program which was implemented on a standard nuclear medicine computer system* with an array processor.† The user is first prompted to move the joystick below the center of its range. This is because the interactive phase of the program is later initiated by having the viewer move the joystick back above its center position. The user is then requested to select the appropriate radionuclide and collimator (4,5), and specify the camera size and magnification which was employed during acquisition. The first frame of the SPECT acquisition set is then passed to the array processor and forward Fast Fourier transformed (FFT'ed) (20). The program then calculates the

FIGURE 1
Flowchart of the interactive visual optimization program.

played. The program then constantly monitors for a change in joystick position and a new filter and image are displayed less than a second after a change in joystick position occurs. Thus the filtering process is under the "real-time" control of the user. Once the user is satisfied with the filtered image, the filter parameters are stored for use in processing the entire SPECT acquisition set by pressing the "M" key of the terminal. All of the acquisition frames are then filtered, and the resulting image set used in the reconstruction of transverse SPECT slices.

RESULTS

Figure 2 illustrates the results of applying the interactive visual optimization program for prereconstruction filtering a ^{99m}Tc liver and spleen SPECT study. The upper portion of each subsection of the figure are the displays presented to the user for different positions of the joystick. The lower portion of each subsection shows a comparison of two transverse slices resulting from the reconstruction of the acquisition image set filtered by the filters of the upper portion. In subsection A, the actual acquisition image, a "soft" Shepp-Logan filter (1,5), and the slices resulting when the Shepp-Logan filter is employed during reconstruction are shown. It should be noted that the Shepp-Logan filter is applied only one-dimensionally during reconstruction of the SPECT slices; whereas, the filters of subsections B–D are applied two-dimensionally, before reconstruction. Subsection A is provided to allow comparison to a standard SPECT filtering method. Subsection B shows the Metz filter and resulting images for the original count-dependent Metz filter formed for this study (4). Subsection C shows these for the Metz filter selected according to the guideline that the filter equal 1.0 at the frequency when the blurred object power spectrum reaches the 90% confidence limit of the noise power spectrum. Note that it is not greatly different from the filter of Figure 2B. This is not surprising since this filter was formed to be optimal in the NMSE sense for an image of the Alderson liver and spleen phantoms. The fourth subsection (D), shows the filter and resulting images for a filter which is over amplifying the noise content of the image (following the inverse filter too far).

A similar set of images is presented in Figure 3 for a ^{99m}Tc bone study. Note that the original count-dependent Metz filter (Fig. 3B) is quite different from that of the visually selected filter (Fig. 3C). The reason for this is that the estimated power spectrum of the blurred object extends to higher frequencies before approaching the level of fluctuations in the noise power spectrum than it did in the liver and spleen study. The coronal and transverse SPECT slices shown in Figure 3 illustrate the improved definition of the anatomy which occurs (in particular, the better contrast between the vertebral bodies and disk spaces in the coronal slice, and visual-

smoothed estimate of the object power spectrum (7), and the a priori "optimal" Metz filter based on MTF, pixel size, and count level. This filter is then displayed overlayed on the normalized logarithm of the estimated blurred object power spectrum as discussed above. The Fourier transform of the image is then multiplied in a circularly symmetric fashion by the filter with the result being stored in a different buffer in the data memory of the array processor (21). This alleviates the need to read the image from disk, pass it to the array processor, and forward FFT it each time the image is filtered. The filtered Fourier transform of the image is inverse FFT'ed, and returned to the host computer for display.
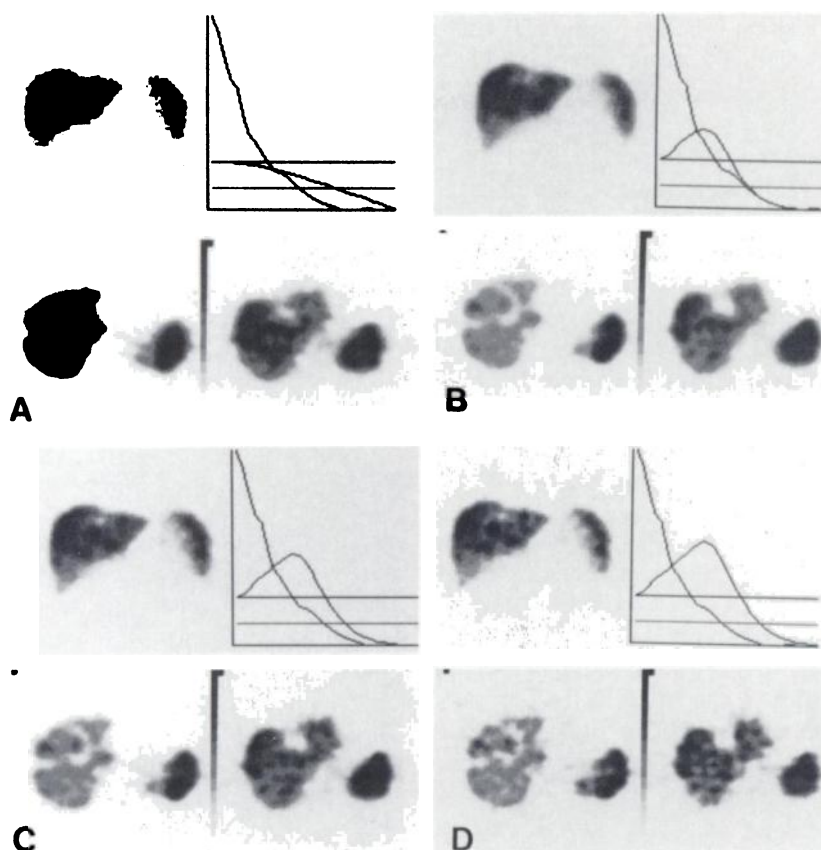
The initial filtered image and filter remain displayed until the user moves the joystick above its central position at which time a new filter and filtered image are calculated and dis-

FIGURE 2
The top of each figure subsection except A contains the filtered SPECT liver and spleen acquisition images with plots of the corresponding filter overlayed on the normalized logarithm of the estimated power spectrum of the blurred object. In subsection A the actual acquisition image is shown along with the filter applied one-dimensionally during reconstruction. The upper horizontal line is drawn at a filter value of 1.0, and the lower horizontal line is the 90% confidence limit for fluctuations in the noise power spectrum. Bottom of each subsection shows two transverse slices reconstructed from acquisition image sets. The slices are from the central and upper portions of the liver, respectively. Filters are: A: Shepp-Logan filter with cutoff frequency equal to the Nyquist frequency. B: original count-dependent Metz. C: Metz judged to be optimal according to our guideline. D: Metz filter visually judged to over-deconvolve the study.
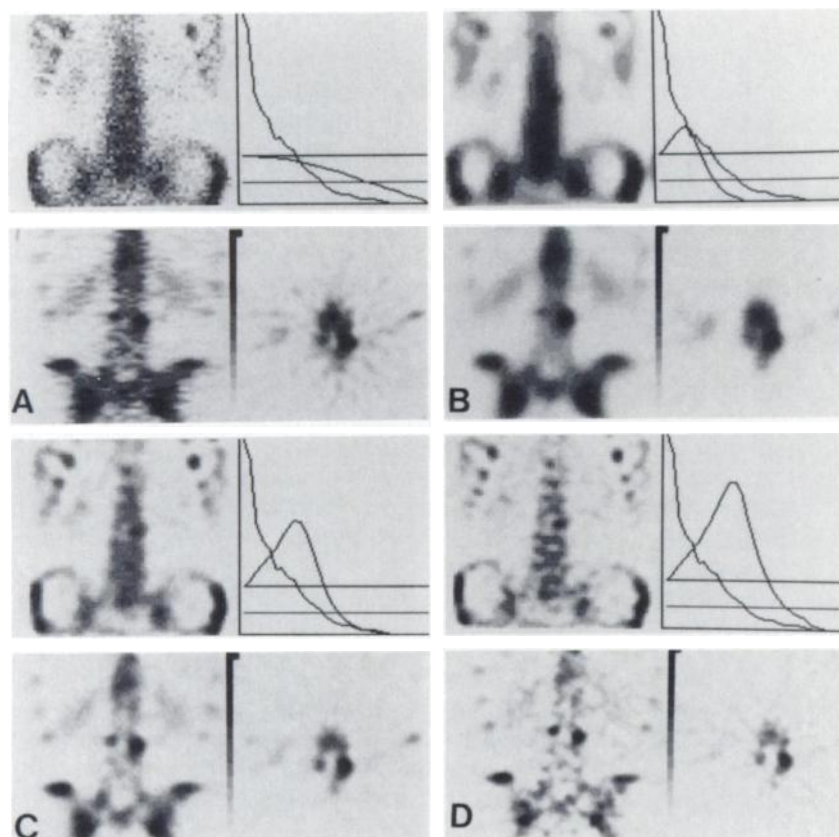
FIGURE 3
The top of each figure subsection except A contains the filtered SPECT bone acquisition images with plots of the corresponding filter overlayed on the normalized logarithm of the estimated power spectrum of the blurred object. In subsection A the actual acquisition image is shown along with the filter applied one-dimensionally during reconstruction. The upper horizontal line is drawn at a filter value of 1.0, and the lower horizontal line is the 90% confidence limit for fluctuations in the noise power spectrum. Bottom of each subsection shows a coronal and a transverse slice reconstructed from each acquisition image set. Filters are: A: Shepp-Logan filter with cutoff frequency equal to the Nyquist frequency. B: Original count dependent Metz. C: Metz judged to be optimal according our guideline. D: Metz filter visually judged to over-deconvolve the study.

ization of the increased uptake associated with a fracture involving the pars) with pre-reconstruction filtering of the SPECT acquisition images with the interactively selected filter.

Figure 4 shows a similar set of images for a thallium-201 perfusion study. The SPECT slices in this case are short-axis views. Notice the improved definition of the left and right ventricular cavities that interactive Metz filtering provides.

Figure 5 provides a comparison of iodine-123-labeled iodamphetamine brain images (5) filtered as in the previous figures. Notice the marked improvement in anatomical definition of both the planar reference image, and SPECT transverse slices which results from joystick optimization of the Metz filter.

DISCUSSION

The guideline which we have developed for filtering SPECT acquisition images to aid in visually selecting an optimal image is to move the joystick (change the pseudo-total count) until the filter has a value of 1.0 when the estimate of the blurred object power spectrum first equals the 90% confidence level for fluctuations in the noise power spectrum. For the count levels of SPECT acquisition images it is necessary to return the filter to near 1.0 at about this frequency to avoid amplifying the noise dominated frequency terms. The

one-dimensionally compressed and filtered power spectrums of Figures 2–5 do not give an idea of the variations at high frequencies caused by noise because they have been "averaged out" in producing the compression (6). A comparison of Figures 1 and 2 of Ref. (6) will make these fluctuations obvious.

The choice of a 90% confidence limit is a heuristic one. However, it seems reasonable as a starting point for visual optimization for images acquired at the count levels typical of SPECT acquisitions. The exact filter judged visually optimal will vary with viewer preference, and object being imaged. Should such variations prove not to be of major importance, then an automatically adaptive, image-dependent version of the Metz filter could be implemented using our proposed guideline.

The criterion which we have used in the past to obtain "optimal" restoration of image quality is the minimization of the normalized mean square error (NMSE). In this paper we are proposing a new criterion, that of user "preference" (7–9). Use of this criterion has led to our proposed guideline which employs the image power spectrum. This method puts the human viewer and his visual system into the optimization process. It has been known for sometime that the two criterion (minimization of the NMSE and observer preference) do not necessarily agree (22–25). This poses the problem as to what is the "best" criterion, especially since these are not the only criteria which may be used for

FIGURE 4
The top of each figure subsection except A contains the filtered ^{201}Tl cardiac perfusion acquisition images with plots of the corresponding filter overlayed on the normalized logarithm of the estimated power spectrum of the blurred object. In subsection A the actual acquisition image is shown along with the filter applied one-dimensionally during reconstruction. The upper horizontal line is drawn at a filter value of 1.0, and the lower horizontal line is the 90% confidence limit for fluctuations in the noise power spectrum. Bottom of each subsection shows short-axis SPECT slices. Filters are: A: Shepp-Logan filter with cutoff frequency equal to the Nyquist frequency. B: Original count dependent Metz. C: Metz judged to be optimal according to our guideline. D: Metz filter visually judged to over-deconvolve the study.
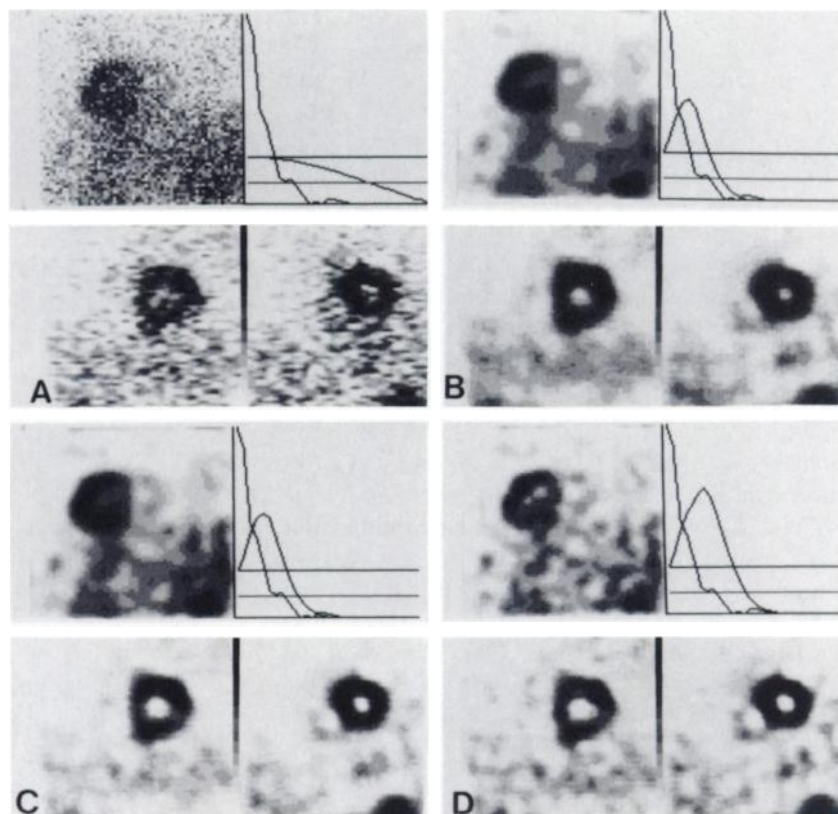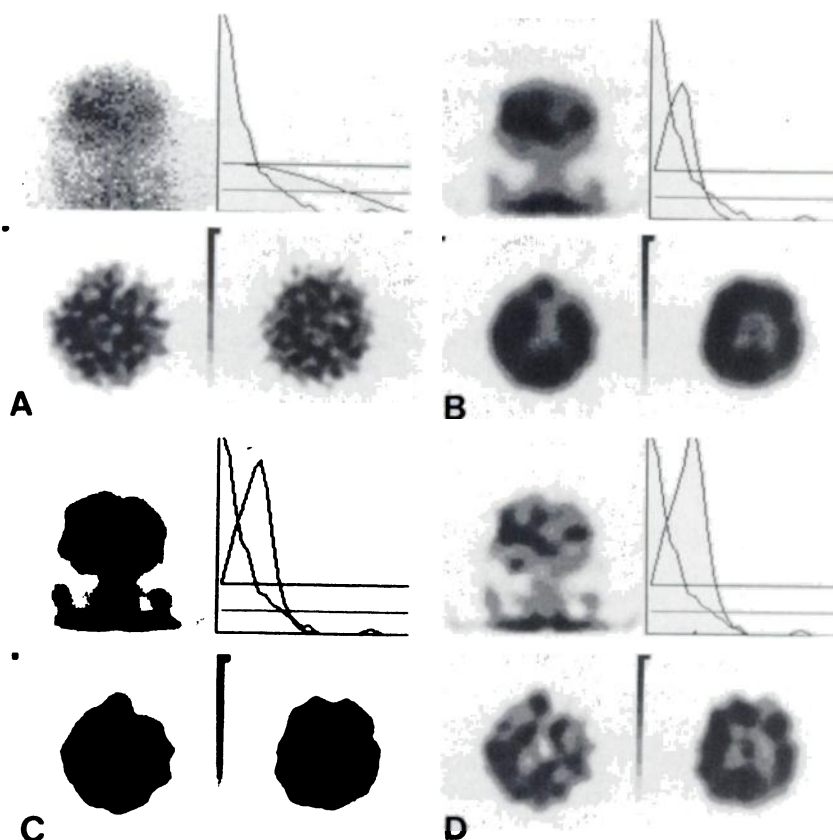
FIGURE 5
The top of each figure subsection except A contains the filtered [^{123}I] iodamphetamine brain acquisition images with plots of the corresponding filter overlayed on the normalized logarithm of the estimated power spectrum of the blurred object. In Subsection A the actual acquisition image is shown along with the filter applied one-dimensionally during reconstruction. The upper horizontal line is drawn at a filter value of 1.0, and the lower horizontal is the 90% confidence limit for fluctuations in the noise power spectrum. Bottom of each subsection shows two transverse SPECT slices. Filters are: A: Shepp-Logan filter with cutoff frequency equal to the Nyquist frequency. B: Original count dependent Metz. C: Metz judged optimal according to our guideline. D: Metz filter visually judged to over-deconvolve the study.

image restoration (*12*). The answer is that there may be no universally "best" criterion in that the choice depends upon the task to be accomplished. That is, lesion detection may require a different criterion from the quantitation of uptake in the lesion. We plan to compare the two criterion we have used through an ROC study to determine if either is better at the task of lesion detection.

The foundation for the use of two-dimensional filtering of SPECT acquisition images is the hypothesis that optimal filtering of the planar acquisition images will result in optimally filtered SPECT slices after reconstruction. This basis for filtering SPECT studies has been observed to work quite well (*1-5*). However, the effects of discrete sampling, angular sampling, the ramp filter, backprojection, and attenuation correction may need to be accounted for in order to obtain SPECT slices which are optimal in a NMSE or visual sense.

To truly have "real-time" visual optimization of SPECT slices one would like to be able to change the filter parameters while viewing the display of a selected SPECT slice. With our present array processor we do not have enough data memory to hold all of the acquisition images (typically 64) in the array processor at one time. The resulting need to store images on disk makes two-dimensional filtering of the acquisition images followed by reconstruction and display of a SPECT slice too time consuming for "real-time" optimization

of filters. Therefore, such an approach was not developed. However, we have implemented software for the interactive filtering of the one-dimensional projection data of a selected SPECT slice while viewing the display of the slice. With this program the projection data for the slice is filtered, and the slice is reconstructed and displayed on the screen less than two seconds after the joystick is moved. It was noted that the quality of the one-dimensionally filtered slices never matched that of the slices when two-dimensionally prereconstruction filtering of the acquisition images was employed. This illustrates the importance of using the data in adjacent slices in an appropriately weighted fashion when reconstructing a SPECT slice. Two-dimensional prereconstruction filtering does this and gains a significant advantage over single slice filtering methods by doing so (*5*).

The MTF used with image restoration was that obtained from a line source at a depth approximately equal to the mean free path of the photons used in imaging (*4,5*). Lacking specific information on the depth of lesions, this seems a reasonable choice. In SPECT imaging the MTF varies much less across a slice than it does with distance away from the collimator in planar imaging (*1*). Thus a reasonable approach would seem to be to determine the MTF postreconstruction, and filter the slices postreconstruction (*1*). It should be noted that three-dimensional filters would be required

if the advantage of using information in the adjacent slices is not to be lost. Such an approach would again be too time consuming, with our present hardware, for the implementation of interactive filtering. Thus this approach was not developed.

In this paper, as well as our past papers, we have formed circularly symmetric filters. The image power spectrum is not circularly symmetric (3). By averaging over the annuli to produce a one-dimensional estimate of the average image power spectrum, the two-dimensional nonsymmetry was lost. In preliminary studies we have determined that use of circularly nonsymmetric Wiener filters based on the actual two-dimensional object power spectrum can significantly reduce the NMSE. It is possible that extension of the joystick control described herein to use with circularly nonsymmetric filters could significantly improve image quality. This has not been tested.

The interactive optimization of a filter under joystick control serves as a good example of the "number crunching" power that an array processor adds to a nuclear medicine computer system. We have also found it a good way to adapt the count-dependent Metz filter to the image being processed, and to serve as an excellent teaching tool on the effects of filtering on image quality.

NOTES

ACKNOWLEDGMENTS

REFERENCES

1. King MA, Schwinger RB, Doherty PW, et al. Two-dimensional filtering of SPECT images using the Metz and Wiener filters. J Nucl Med 1984; 25:1234–1240.
2. Webb S, Long AP, Ott RJ, et al. Constrained deconvolution of SPECT liver tomograms by direct digital image restoration. Med Phys 1985; 12:53–58.
3. Madsen MT, Park CH. Enhancement of SPECT images by Fourier filtering the projection image set. J Nucl Med 1985; 26:395–402.
4. King MA, Schwinger RB, Penney BC. Variation in the count-dependent Metz filter with imaging system MTF. Med Phys 1986; 13:139–149.
5. King MA, Schwinger RB, Penney BC, et al. Digital restoration of In-111 and I-123 SPECT images with optimized Metz filters. J Nucl Med 1986; 27:1327–1336.
6. King MA, Doherty PW, Schwinger RB, et al. A Wiener filter for nuclear medicine images. Med Phys 1983; 10:876–880.
7. MacAdam DP. Digital image restoration by constrained deconvolution. J Opt Soc Amer 1970; 60:1617–1627.
8. Boulter JF. Interactive digital image restoration and enhancement. Comp Graph Image Process 1979; 11:301–312.
9. Miller TR, Rollins ES. A practical method of image enhancement by interactive digital filtering. J Nucl Med 1985; 26:1075–1080.
10. Sebern MJ, Horgan JD, Meade RC, et al. Minicomputer enhancement of scintillation camera images. J Nucl Med 1976; 17:647–652.
11. Huang TS, Burnett JW, Deczky AG. The importance of phase in image processing filters. IEEE Trans Acoust Speech Signal Proces 1975; 23:529–542.
12. Andrews HC, Hunt BR. Digital image restoration. Englewood Cliffs, NJ: Prentice-Hall, Inc., 1977: 81–82, 126–208.
13. Jenkins GM, Watts DG. Spectral analysis and its applications. San Francisco: Holden-Day, 1968: 6–8, 230–234.
14. Goodman JW, Belsher JF. Fundamental limitations in linear invariant restoration of atmospherically degraded images. In Imaging through the atmosphere, SPIE, Vol. 75, Society of Photo-Optical Instrumentation Engineers, 1976, 141–154.
15. Kirch DL, Brown DW. Nonlinear frequency domain techniques for enhancement of radionuclide images. In Information processing in scintigraphy. USERDA Conf-730687, 1973, 102–114.
16. Madsen MT. Signal to noise requirements for the perception of sinusoidal components in digital nuclear medicine images [Abstract]. Med Phys 1985; 12:527.
17. King MA, Doherty PW, Schwinger RB, et al. Fast count-dependent digital filtering of nuclear medicine images: concise communication. J Nucl Med 1983; 24:1039–1045.
18. Metz CE. A mathematical investigation of radioisotope scan image processing. Ph.D. Thesis, University of Pennsylvania, 1969.
19. Metz CE, Beck RN. Quantitative effects of stationary linear image processing on noise and resolution of structure in radionuclide images. J Nucl Med 1975; 15:164–170.
20. Brigham EO. The fast fourier transform. Englewood Cliffs, NJ: Prentice-Hall, 1974: 148–171.
21. King MA, Doherty PW, Rosenberg RJ, et al. Array processors: an introduction to their architecture, software, and application in nuclear medicine. J Nucl Med 1983; 24:1072–1079.
22. Mannos JL, Sakrison DJ. The effects of a visual fidelity criterion on the encoding of images IEEE Trans Inf Theory 1974; 20:525–536.
23. Pratt WK. Digital image processing. Englewood Cliffs, NJ: Prentice-Hall, 1978: 174–182.
24. Cannon TM, Trussell HJ, Hunt BR. Comparison of image restoration methods. Appl Optics 1978; 17:3384–3390.
25. Hentea TA, Algozi VR. Perceptual models and the filtering of high-contrast achromatic images. IEEE Trans Sys Man Cyber 1984; 14:230–246.